Journal of Power Sources 236 (2013) 95–102

Contents lists available at SciVerse ScienceDirect

Journal of Power Sources

journal homepage: www.elsevier.com/locate/jpowsour

Short communication

Study of the two-step W/WO_3 solar to fuel conversion cycle for syngas production

Jarrod D. Milshtein [a,b], Eric Gratz [b], Soumendra N. Basu [a,b], Srikanth Gopalan [a,b], Uday B. Pal [a,b,*]

[a] Boston University, Department of Mechanical Engineering, 110 Cummington St., Boston, MA 02215, USA
[b] Boston University, Division of Materials Science and Engineering, 15 Saint Mary's St., Brookline, MA 02446, USA

HIGHLIGHTS

- We propose the W/WO_3 redox cycle for solar syngas production.
- Solar heat will be used to produce $H_{2(g)}$ and $CO_{(g)}$.
- High gravimetric fuel productivity of the system is demonstrated.
- High solar to fuel conversion efficiencies are possible.
- Complete thermodynamic and kinetic description is supplied.

ARTICLE INFO

Article history:
Received 13 October 2012
Received in revised form
11 February 2013
Accepted 13 February 2013
Available online 27 February 2013

Keywords:
Syngas
Hydrogen
Solar concentrator
Tungsten
Thermochemical cycles
Water splitting

ABSTRACT

This work proposes syngas production by utilizing the W/WO_3 redox system in a solar-powered two-step thermochemical cycle. Three chemical reactions occur in two chambers of a solar concentrator. A high temperature reaction reduces WO_3 powder to metallic tungsten in both the chambers. Subsequently, the temperature of the first chamber is lowered and $H_{2(g)}$ is produced via re-oxidation of the tungsten powder using $H_2O_{(g)}$. The temperature of the second chamber is simultaneously lowered to an intermediate temperature, and $CO_{2(g)}$ oxidizes the tungsten powder to generate $CO_{(g)}$. The gas streams coming out of the two chambers will be combined, resulting in syngas production. Complete thermodynamic and kinetic analyzes of the system are described in this paper. The W/WO_3 redox cycle offers greater gravimetric fuel productivity compared to previously proposed systems, and the entire cycle can be operated in the solid phase. Conditions to prohibit tungsten volatilization and tungsten carbide formation are also outlined.

1. Introduction

Solar energy offers an abundant power source radiating the earth with many times more energy than currently consumed by the entire world population [1]. Another motivation to move toward solar energy is to reduce carbon dioxide emissions from fossil fuel combustion. The inherent issue with solar energy is that solar radiation cannot be stored directly, as other forms of energy can. Intermittency of solar energy also yields difficulty in supplying a continuous and reliable energy alternative to traditional fossil fuels [2]. Thus a method of storing the sun's energy is imperative to a successful transition toward a solar-based energy economy. Storage of electrical energy produced by photovoltaics has been proposed by storing the energy in batteries or by storing the electrical energy mechanically in pumped hydro [1].

This study proposes a new two-step metal/metal-oxide thermochemical cycle for $H_{2(g)}$ and $CO_{(g)}$ production using solar heat. Simple thermochemical cycling of metal oxides for fuel production relies on a two-step process in which first a lower temperature reaction oxidizes a metal via oxygen transfer from $H_2O_{(g)}$ or $CO_{2(g)}$. This step produces storable and transportable $H_{2(g)}$ or $CO_{(g)}$. Second, a high temperature reaction reduces a metal oxide via an endothermic reaction [3]. The cycle for $H_{2(g)}$ and $CO_{(g)}$ production via $H_2O_{(g)}$ and $CO_{2(g)}$ reduction, is shown below in Equation (1)–(5).

Low Temperature, T_L:

$$M + xH_2O_{(g)} \rightarrow MO_x + xH_{2(g)} \quad (1)$$

Intermediate Temperature, T_I:

$$M + xCO_{2(g)} \rightarrow MO_x + xCO_{(g)} \quad (2)$$

* Corresponding author. Boston University, Department of Mechanical Engineering, 110 Cummington St., Boston, MA 02215, USA. Tel.: +1 6173537708; fax: +1 6173535548.
E-mail address: upal@bu.edu (U.B. Pal).

0378-7753/$ – see front matter © 2013 Elsevier B.V. All rights reserved.
http://dx.doi.org/10.1016/j.jpowsour.2013.02.038

High Temperature, T_H:

$$MO_x \rightarrow M + \frac{x}{2}O_{2(g)} \quad (3)$$

Total cycle:

$$H_2O_{(g)} \rightarrow H_{2(g)} + \frac{1}{2}O_{2(g)} \quad (4)$$

$$CO_{2(g)} \rightarrow CO_{(g)} + \frac{1}{2}O_{2(g)} \quad (5)$$

Such a two-step thermochemical cycle was first published by Nakamura in 1977, utilizing the FeO/Fe_3O_4 system [4]. Although Nakamura was not the first to propose thermochemical cycling for generating hydrogen gas from solar energy via water dissociation, he was the first to find a suitable two-step reaction system [5]. Nakamura's proposed system, however, was deemed impractical due to very high operating temperatures. Cobalt, nickel, zinc, manganese, titanium, and ceria based thermochemical systems were later proposed as alternatives to Nakamura's system [3,5–8]. The ideal system must utilize materials stable at high temperatures, and the ideal system should also have high gravimetric fuel productivity [3].

This study presents a theoretical analysis for the viability of a tungsten/tungsten-oxide (W/WO_3) based thermochemical system for solar to fuel conversion. The proposed W/WO_3 system offers higher gravimetric fuel productivity than similarly proposed systems and can operate at much lower temperatures. Such a system will require two reaction chambers, one for $H_{2(g)}$ production and a second for $CO_{(g)}$ production. Figs. 1 and 2 are flow charts depicting the thermochemical cycles taking place. A schematic of the two reaction chamber solar concentrator is shown in Fig. 3.

Since the system can be operated below the melting point of WO_3, the cycle will utilize a porous powder bed of W/WO_3. The porous powder bed will increase reaction kinetics. In the analysis description, the W/WO_3 cycle will occasionally be compared to the ceria based cycle proposed by Chueh and Haile [3]. The ceria based cycle offers a suitable comparison because the ceria cycle also operates entirely in the solid phase and has been examined for syngas production. Other cycles have only considered $H_{2(g)}$ production or operate in the liquid/vapor phases. For example, the Zn/ZnO system is a thermochemical cycle for syngas production which involves a quenching step to re-solidify Zn vapor produced during the cycle [9]. Also, the cycle requires the use of Zn nanoparticles for the lower temperature oxidation reactions to occur sufficiently fast, leading to a more complex system than the tungsten or ceria based cycles [10].

The W/WO_3 system has not yet been studied experimentally for this application, but the same cycle has been proposed for an energy storage system to be used in conjunction with solid oxide fuel cells [11]. This analysis considers the theoretical thermodynamic and kinetic capabilities of the W/WO_3 system to produce $H_{2(g)}$ and $CO_{(g)}$ from $H_2O_{(g)}$ and $CO_{2(g)}$, respectively. Operating conditions to avoid the volatilization of tungsten and its oxides are also discussed.

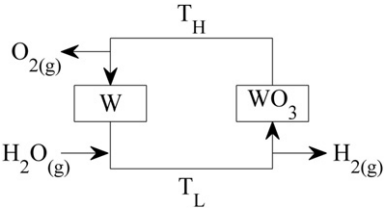

Fig. 1. Flow chart depicting the production of $H_{2(g)}$ during the thermochemical cycle.

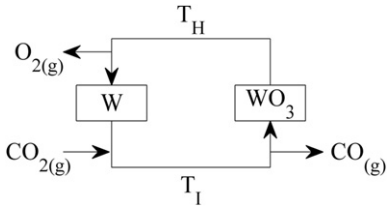

Fig. 2. Flow chart depicting the production of $CO_{(g)}$ during the thermochemical cycle.

2. Thermodynamics

2.1. Characteristics of redox reactions of the W/WO_3 system

Tungsten oxidation has been notoriously difficult to study resulting in discrepancies among peer-reviewed journals throughout decades of research. Specifically, reports have varied in the discussion of kinetics, composition, and structure of the tungsten oxide formations. As difficult as the oxidation mechanism has been to study, the tungsten oxidation sequence is typically accepted as follows: $W \rightarrow WO_2 \rightarrow WO_{2.72} \rightarrow WO_{2.96} \rightarrow WO_3$ [12]. The reduction sequence is exactly opposite [11]. The stability of the intermediate oxides depends on a critical oxygen partial pressure (pO_2^{cr}) above which the oxide will advance to the next higher oxide, and pO_2^{cr} can be determined from the reaction constant for the oxidation reaction. Using *HSC Chemistry* software a phase stability diagram was generated as a function of temperature and oxygen partial pressure [13]. The phase stability diagram is shown in Fig. 4. Critically, in order for WO_3 to be reduced to W at high temperature, the pO_2 must be below pO_2^{cr} for W formation at a given reaction temperature. Low oxygen partial pressures will be obtained by passing inert gas such as $Ar_{(g)}$.

During the analysis of the W/WO_3 cycle for syngas production, temperatures up to the melting point of WO_3 (1643 K) were initially considered as possible reaction temperatures. The melting point of tungsten trioxide presented the upper limit operating temperature because it has the lowest melting point of all the solid phases in the W–O system. As the proposed system takes advantage of porous tungsten and tungsten oxide powders, melting of the powders must be avoided to prevent solidification and densification of the powder bed.

2.2. Gravimetric fuel productivity

An integral first step to examining the viability of a thermochemical cycle for fuel production is determining the gravimetric fuel productivity for that cycle. The gravimetric fuel productivity

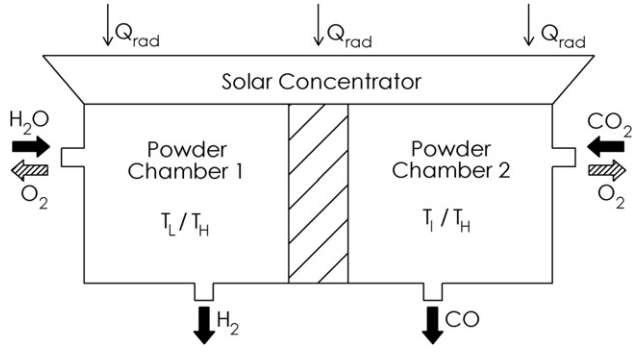

Fig. 3. Schematic of the two reaction chamber solar concentrator apparatus for syngas production using the W/WO_3 thermochemical system.

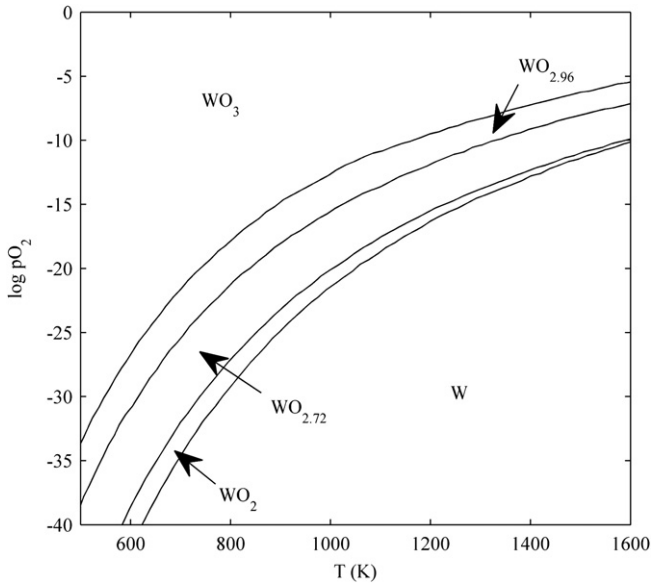

Fig. 4. Phase stability diagram of the W–O–H system as a function of pO_2 and temperature. pH_2 is fixed at 10^{-20}. Diagram was generated using *HSC Chemistry*.

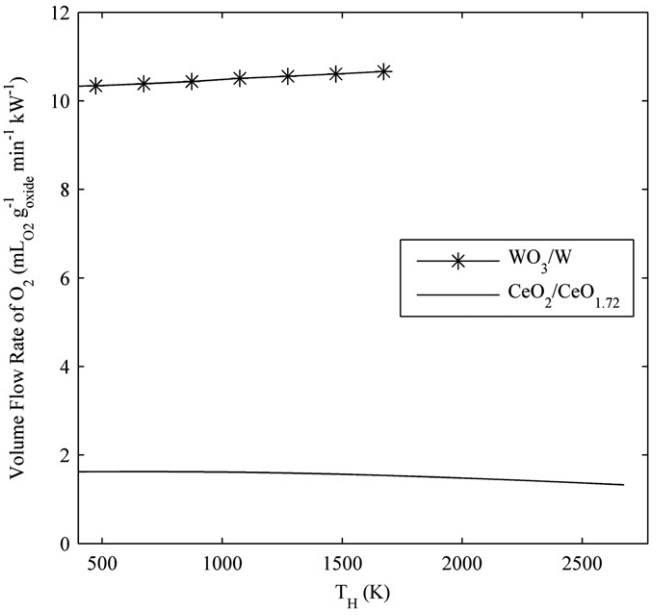

Fig. 5. Maximum volumetric $O_{2(g)}$ release rate for the WO_3/W and $CeO_2/CeO_{1.72}$ reduction steps as functions of temperature. Values are plotted for the temperature range of 400 K to the melting point of the oxides.

refers to the amount of fuel that can be produced per gram of oxide per unit solar power. The simplest way to demonstrate this concept quantitatively is to determine how much oxygen can be removed during the high temperature reduction of WO_3 per gram per unit incident solar radiation. In short, high oxygen removal rates per gram of WO_3 per unit solar power are desirable. The moles of oxygen released during reduction of the oxide is directly proportional to the moles of fuel that can be produced during oxidation of the metal. The higher the oxygen removal rate per gram per unit solar power, the less oxide material required to produce a given amount of fuel and the more efficiently the solar energy can be stored as fuel. The discussion of solar to fuel conversion efficiency will be continued in Section 2.4.

Assuming a nominal solar power of 1 kW, the maximum attainable volumetric flow rate of oxygen was calculated for the reduction of WO_3 to W per unit mass of WO_3. Reactions were assumed to occur isothermally, and the energy required to heat the system to the reaction temperature was neglected. The same calculation was performed for the recently proposed ceria based system as a comparison, assuming that $CeO_{1.72}$ is produced as the lower oxide for that system. Oxygen produced was assumed to be removed from the system immediately after production. Finally, the kinetic and potential energy of the gases were also assumed to be negligible. With the above assumptions, Equation (6) was derived from the First Law to define the volumetric flow rate of oxygen gas per gram of reactant oxide per kW solar power. In Equation (6), $\dot{V}_{O_2^{STP}}$ is the volume flow rate of oxygen in mL min^{-1} kW^{-1} g_{oxide}^{-1} at STP, ΔH_{rxn} is the enthalpy change for the reduction reaction in kJ mol^{-1}, $n_{O_2^{STP}}$ is the moles of oxygen produced from the reaction, n_{oxide} is the number of moles of oxide reduced during the reaction, and MW_{oxide} is the molecular weight of the oxide in g mol^{-1}. The calculated flow rates are plotted in Fig. 5.

$$\dot{V}_{O_2^{STP}} = 1344 \cdot 10^3 \cdot \frac{1}{\Delta H_{rxn}} \cdot \frac{n_{O_2^{STP}}}{n_{oxide}} \cdot \frac{1}{MW_{oxide}} \frac{mL}{g_{oxide} \cdot min \cdot kW} \quad (6)$$

As shown in Fig. 5, the volumetric $O_{2(g)}$ release rate is almost an order of magnitude higher in the WO_3 W^{-1} reduction reaction than in the reduction of CeO_2 to $CeO_{1.72}$. The improvement of the W/WO_3 cycle in gravimetric fuel productivity over the recently demonstrated ceria based cycle shows that the W/WO_3 cycle has a potentially competitive advantage.

2.3. Fuel production reactions

The feasibility of tungsten as a thermochemical reductant for $H_2O_{(g)}$ and $CO_{2(g)}$ was considered by analyzing the free energy change of the reactions in Equations (7) and (8) as a function of temperature. The free energy changes as a function of temperature are plotted in Fig. 6.

$$W + 3H_2O_{(g)} \rightarrow WO_3 + 3H_{2(g)} \quad (7)$$

$$W + 3CO_{2(g)} \rightarrow WO_3 + 3CO_{(g)} \quad (8)$$

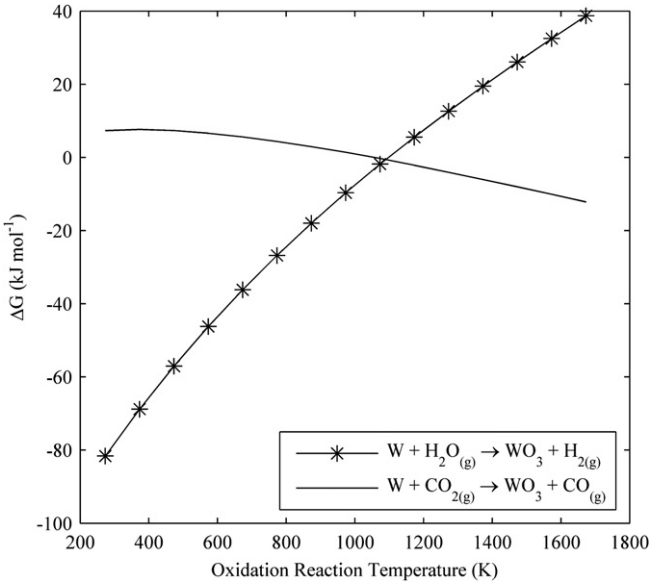

Fig. 6. Free energy change for the oxidation of tungsten by $H_2O_{(g)}$ and $CO_{2(g)}$ as a function of temperature.

Again, reaction temperatures up to the melting point of WO_3 were initially considered as possible oxidation reaction temperatures. Oxidation by $H_2O_{(g)}$ is favorable below 1073 K while at temperatures above 1073 K, oxidation by $CO_{2(g)}$ becomes favorable. Hence, low temperature (T_L) and intermediate temperature (T_I) reaction chambers have been selected for the separate production of $H_{2(g)}$ and $CO_{(g)}$, respectively. Separating the chambers also prevents the synthesis of hydrocarbons, such as methane, during tungsten oxidation. Oxidation by $H_2O_{(g)}$ below 1073 K is an exothermic reaction, and the $H_{2(g)}$ production rate can be described by the amount of $H_{2(g)}$ formed per kJ of heat rejected. The volumetric release rate is described by Equation (9), where $\dot{V}_{H_2^{STP}}$ is the volume flow rate of hydrogen in mL kJ^{-1} g_{oxide}^{-1} at STP, ΔH_{rxn} is the enthalpy change for the oxidation reaction in kJ mol^{-1}, $n_{H_2^{STP}}$ is the moles of hydrogen produced from the reaction, n_{oxide} is the number of moles of oxide reduced during the reaction, MW_{oxide} is the molecular weight of the oxide in g mol^{-1}. The volumetric release rate is plotted as a function of temperature in Fig. 7.

$$\dot{V}_{H_2^{STP}} = 22.4\cdot 10^3 \cdot \frac{1}{-\Delta H_{rxn}} \cdot \frac{n_{H_2^{STP}}}{n_{oxide}} \cdot \frac{1}{MW_{oxide}} \quad \frac{mL}{g_{oxide}\cdot kJ} \tag{9}$$

Contrastingly, oxidation by $CO_{2(g)}$ above 1073 K is a slightly endothermic reaction, and thus heat from the solar concentrator is required for the reaction to proceed. The maximum attainable rate of isothermal $CO_{(g)}$ production via tungsten oxidation can be calculated in the same manner as the maximum oxygen evolution rate previously determined in Section 2.2. The results are plotted in Fig. 8.

2.4. Cycle efficiencies

The thermodynamic cycle efficiency for fuel production can be described as the ratio of the higher heating value (HHV) of the output fuel to the solar heat energy (Q_{solar}) input to the cycle, as shown in Equation (10), where η_{solar} is the solar to fuel conversion efficiency, n_{fuel} is the number of moles of fuel produced during the reaction, HHV is the higher heating value of the fuel, and Q_{solar} is the solar heat energy input to the cycle. Equations (11) and (12) show the quantity of solar heat energy input to the cycle considering the energy needed to heat reactant gases to T_L or T_I, to heat tungsten oxide to T_H, and for endothermic reactions to occur. Heat rejected from exothermic reactions was also considered. In Equations (11) and (12), η_{abs} is the ideal blackbody cavity absorption for a concentrated solar flux of 5 MW m^{-2}, C_{p,WO_3} is the specific heat of WO_3, and ΔH_{red} is the heat energy required to reduce WO_3 to W. In Equation (11), n_{H_2O} is the number of moles of $H_2O_{(g)}$ consumed during the reaction, $\Delta H_{H_2O(l)\rightarrow(g)}^{298\ K\rightarrow 373\ K}$ is the energy required to vaporize 1 mol of $H_2O_{(l)}$, $C_{p,H_2O_{(g)}}$ is the specific heat of $H_2O_{(g)}$, and ΔH_{oxy} is the heat released during tungsten oxidation with $H_2O_{(g)}$. In Equation (12), n_{CO_2} is the number of moles of $CO_{2(g)}$ consumed, $C_{p,CO_{2(g)}}$ is the specific heat of $CO_{2(g)}$, and ΔH_{oxy} is the heat energy required to oxidize tungsten with $CO_{2(g)}$.

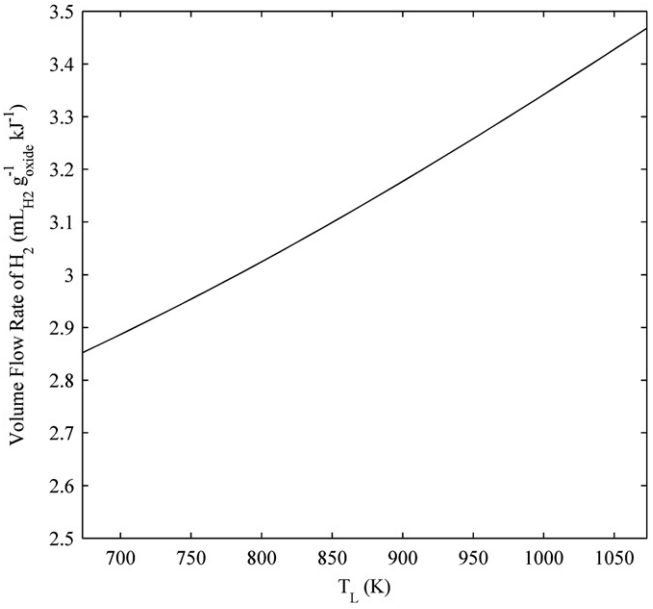

Fig. 7. Volumetric $H_{2(g)}$ release rate for the $W + 3H_2O_{(g)} \rightarrow WO_3 + 3H_{2(g)}$ reaction as a function of temperature per kJ of heat energy rejected. Values are plotted for the temperature range of 673 K–1073 K.

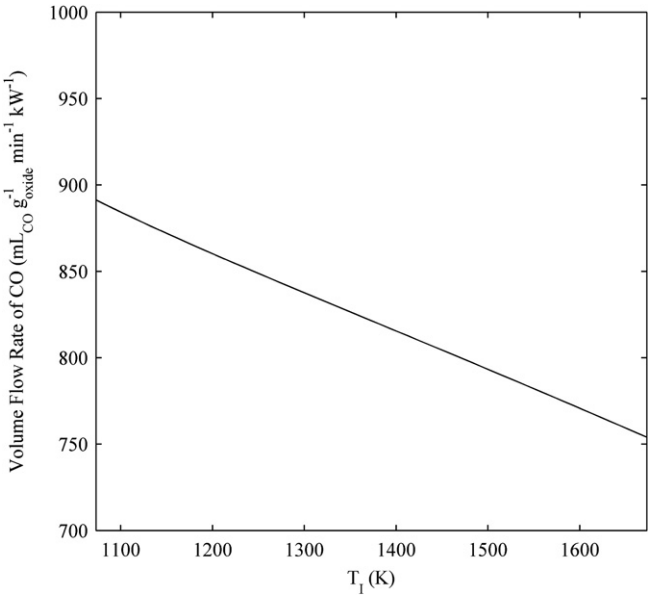

Fig. 8. Maximum volumetric $CO_{(g)}$ release rate for the $W + 3CO_{2(g)} \rightarrow WO_3 + 3CO_{(g)}$ reaction as a function of temperature. Values are plotted for the temperature range of 1073 K to the melting point of WO_3.

$$\eta_{solar} = n_{fuel}\cdot\frac{HHV}{Q_{solar}} \tag{10}$$

$$Q_{solar-H_2O} = \frac{1}{\eta_{abs}}\cdot\left[n_{H_2O}\cdot\left(\Delta H_{H_2O(l)\rightarrow(g)}^{298\ K\rightarrow 373\ K} + \int_{373K}^{T_L} C_{p,H_2O_{(g)}}\,dT\right) + \Delta H_{oxy} + \int_{T_L}^{T_H} C_{p,WO_3}\,dT + \Delta H_{red}\right] \tag{11}$$

$$Q_{solar-CO_2} = \frac{1}{\eta_{abs}}\cdot\left[n_{CO_2}\cdot\int_{298K}^{T_L} C_{p,CO_{2(g)}}\,dT + \Delta H_{oxy} + \int_{T_L}^{T_H} C_{p,WO_3}\,dT + \Delta H_{red}\right] \tag{12}$$

This efficiency description was previously selected by Chueh and Haile to describe the ceria based system [3]. Thus, the W/WO_3 cycle efficiency can be directly compared to the ceria cycle

efficiency. Calculations were performed on the molar basis of the oxide. The HHV of $H_{2(g)}$ was taken to be 285.8 kJ mol^{-1}. The HHV of $CO_{(g)}$ was simply the enthalpy of combustion of $CO_{(g)}$ at STP, which was taken to be 257.2 kJ mol^{-1}. The solar to fuel energy conversion efficiency is ultimately a function of the cycle reaction temperatures, T_L, T_I, and T_H. Cycle efficiencies as a function of these temperature variables are shown in Fig. 9. As a comparison, the cycle efficiencies using the ceria based system from Chueh et al. have also been plotted as a function of T_L and T_H in Fig. 9.

When the W/WO_3 cycle efficiencies are compared to Chueh's ceria based system, the W/WO_3 cycle appears even more attractive; efficiencies are approximately 2.5 times higher for the W/WO_3 system. The conversion of $H_2O_{(g)}$ to $H_{2(g)}$ reaches efficiencies up to 95 % while the $CO_{(g)}$ generation cycle reaches 86 % efficiency. The efficiencies shown for the ceria system are even likely to be overestimates, as an upper value of $\delta_{oxygen} = 0.28$ was assumed for all temperatures. In reality, δ changes with temperature. Chueh and Haile, in fact, reports up to only 22 % efficiency for the ceria based system [3].

As demonstrated by Equations (11) and (12), efficiency calculations did not consider heat recapturing. Heat removed from the system during the high temperature reaction could be captured using a heat exchanger and heat from the intermediate temperature reaction chamber could be directed into the low temperature reaction chamber during cycle operation. If these heat capturing methods are employed, the cycle efficiency would increase even higher. Also notably, the W/WO_3 cycle efficiency only varies by a few percent across a wide range of possible operating temperatures. This result indicates that operating conditions to maximize reaction kinetics and minimize volatility will not greatly affect the cycle efficiency.

2.5. Avoiding tungsten carbide formation

Formation of tungsten carbide (WC) during the oxidation of tungsten by $CO_{2(g)}$ should be avoided for two reasons. First, the formation of this material should be avoided to take full advantage of the 3:1 oxygen to tungsten stoichiometry of tungsten trioxide, which is the source of the cycle's high gravimetric fuel productivity. Second, this material should be avoided to prevent release of $CO_{2(g)}$ during oxidation reactions. By analyzing the phase stability diagram of the tungsten–carbon–oxygen system, it is possible to find a pCO/pCO_2 ratio for which WO_3 is the stable tungsten species. The phase stability diagram for the W–C–O system at 1073 K is shown in Fig. 10. The temperature of 1073 K represents the lowest possible operating temperature for the production of $CO_{(g)}$. As temperature increases, the stable region of WO_3 grows larger. During operation of the solar concentrator, pCO/pCO_2 ratios will be maintained to ensure that WC is not formed.

3. Kinetics

3.1. Gas–solid reaction mechanism

The proposed thermochemical system will utilize a W/WO_3 powder bed in which a gas–solid reaction will occur. In a fixed and isothermal powder bed, the reaction takes place as a moving front. The gas–solid reaction can be assumed to have the general form shown in Equation (13), in which A is the reactant gas and B is a loosely packed, powdered solid [11].

$$A_{(g)} + bB_{(s)} \rightarrow eE_{(g)} + fF_{(s)} \tag{13}$$

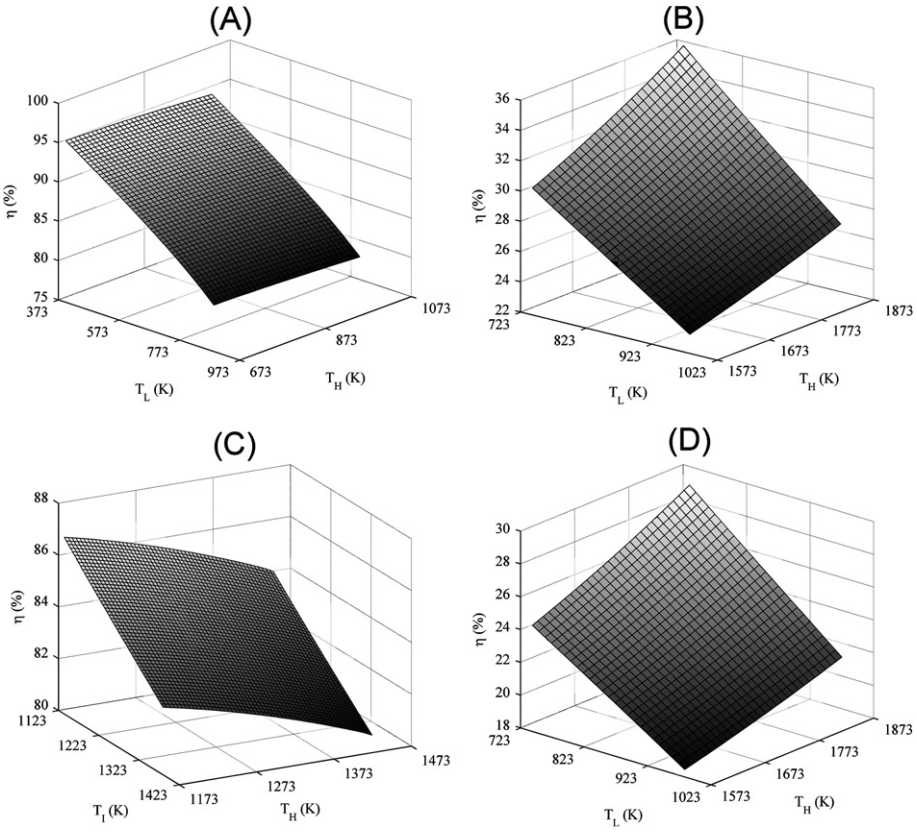

Fig. 9. (A) W/WO_3 cycle efficiency for hydrogen gas production as a function of T_L and T_H. (B) Ceria cycle efficiency for hydrogen gas production as a function of T_L and T_H. (C) W/WO_3 cycle efficiency for carbon monoxide gas production as a function of T_I and T_H. (D) Ceria cycle efficiency for carbon monoxide gas production as a function of T_L and T_H.

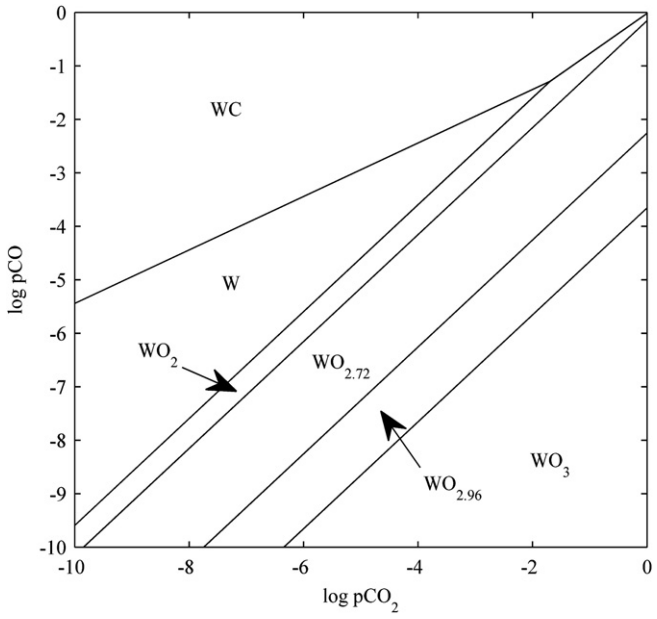

Fig. 10. Phase stability diagram of the W–C–O system as a function of pCO_2 and pCO. Temperature is fixed at 1073 K. Diagram was generated using *HSC Chemistry*.

The reaction takes place by forming a thin layer of the solid product F, which is also a powder. Due to the porous nature of the thin powder layer, reactant gas A diffuses through the product layer and reacts at the new interface between reactant B and product F. Importantly, the reaction front is assumed to maintain a planar geometry as it moves through the powder bed, and this behavior has been experimentally verified [11]. The density of the solid product and solid reactant are also assumed to be the same, and the rate that the reaction front proceeds is assumed to be small compared to the gas diffusion of reactant gas A through the powder bed; the diffusion of the product gas $E_{(g)}$ is considered to be very rapid and not rate controlling [11].

3.2. Rate controlling step

The molar rate of gas reactant loss in a gas–solid reaction can be written as a function of three resistances: reactant gas diffusion through the gaseous boundary layer, diffusion of the reactant gas through the solid, and the chemical reaction rate constant. Equation (14) illustrates the relationship between molar rate of gas reactant loss, where S_{ex} is the surface area of the powder bed exposed to the gas, $d\overline{N}_A/dt$ is the molar rate of consumption of reactant gas A, C_A is the concentration of reactant gas A, k_g is the gas phase mass transfer coefficient, R is the radius of curvature of the powder bed, D_e is the diffusion coefficient of reactant gas A in the solid product F, and k'' is the chemical reaction rate constant [14].

$$\frac{-1}{S_{ex}}\cdot\frac{d\overline{N}_A}{dt} = \frac{C_A}{\frac{1}{k_g}+\frac{R}{2D_e}+\frac{1}{k''}} \tag{14}$$

By comparing the relative magnitudes of $1/k_g$, $R/(2D_e)$, and $1/k''$, the most resistive segment of the reaction process can be determined. If the most resistive segment is much more resistive that the other two segments, the most resistive segment will control the rate of the reaction.

A W/WO_3 powder bed similar to the one described by Haboury et al., will be employed for the thermochemical cycle proposed in this study. In that study, powder particles in the size range of 10 μm–20 μm were used [11]. The particle size of 10 μm will be assumed in this study to form an argument for the rate limiting step of the gas–solid reaction. For such a system it has been shown that when the gas flow rate is sufficiently high and the bed height is not significantly large, the velocity of the moving front is chemical reaction controlled [11]. Therefore the reaction rate in Equation (14) can be simplified to Equation (15).

$$\frac{-1}{S_{ex}}\cdot\frac{d\overline{N}_A}{dt} = C_A k'' \tag{15}$$

Prior studies on the oxidation of tungsten by $H_2O_{(g)}$ and $CO_{2(g)}$ have reported on the reaction rates of these oxidation reactions. Oxidation by $CO_{2(g)}$, however, has been studied more extensively than oxidation by $H_2O_{(g)}$. The reaction rate of the reduction reaction of tungsten oxide during the high temperature reaction is also important. Studies on tungsten oxide reduction by passing inert gas in the temperature range of interest were not found during literature review; tungsten oxide reduction has been typically studied using hydrogen as a reductant [11,15]. It would be expected, though, that the reaction rate of the high temperature reaction would increase with both temperature and purity of the inert gas.

Sabourin and Yetter determined an Arrhenius fit for the chemical reaction rate constant of tungsten oxidation by $CO_{2(g)}$ [16]. The relationship is provided in Equation (16), where k_{CO_2} is the reaction rate in m s^{-1}, R is the gas constant given in cal K^{-1} mol^{-1}, T is temperature, and P_{CO_2} is the $CO_{2(g)}$ pressure in torr. The relationship in Equation (16) has been modified slightly from its original publication for consistency of units. Sabourin reported his reaction rate constant values in units of mol m^{-2} s^{-1}, so the original values were divided by the molecular density of tungsten to achieve units of m s^{-1} (meters per second). The same study also supplied an Arrhenius fit to incorporate the effect of $CO_{(g)}$ pressure (P_{CO}) on oxidation kinetics, as it was found that with increased P_{CO}, reaction rates decreased [16]. Notably, another study has also reported the same effect of P_{CO} on reaction rate [17]. As the thermochemical cycle for $CO_{(g)}$ production using the W/WO_3 system has not yet been tested experimentally, it is difficult to estimate P_{CO} in the reaction chamber. In trying to determine the rate limiting step of the reaction by $CO_{2(g)}$ oxidation, the effect of P_{CO} was not considered. From the reaction rate constant, it is possible to estimate the oxidation rate of tungsten by $CO_{2(g)}$ in the temperature range of interest using Equation (15).

$$k_{CO_2} = .0272\cdot\exp\left[\frac{-64000}{RT}\right]\cdot\left[P_{CO_2}\right]^{0.6} \text{ m s}^{-1} \tag{16}$$

During a literature search, only one extensive study was located that reported on the production of $H_{2(g)}$ via the oxidation of tungsten by $H_2O_{(g)}$. This study provided the gas production rate as a function of temperature in the range of 673 K–1473 K, which is shown in Equation (17), where k_{H_2O} is the reaction rate and T is temperature [18]. Again, this relationship has been modified for unit consistency. Employing this reaction rate constant, it is possible to estimate the oxidation rate of tungsten by $H_2O_{(g)}$ in the temperature range of interest using Equation (15).

$$k_{H_2O} = 2.135\cdot10^{-3}\cdot\exp\left[\frac{-16720}{T}\right] \text{ m s}^{-1} \tag{17}$$

4. Volatility

The volatility of tungsten metal and the tungsten oxides must be controlled to ensure that there is no loss of powder bed by vapor phase removal. Possible volatility mechanisms would include the sublimation of tungsten and its oxides or by reaction with $H_2O_{(g)}$ to

form a volatile tungsten hydroxide compound. Tungsten and its oxides do not form new volatile compounds during oxidation by $CO_{2(g)}$ [16]. No literature was found that reported volatility in $CO_{(g)}$ either. The possible volatilization pathways were investigated through literature review and thermodynamic analysis. Operating conditions to minimize volatility are proposed.

4.1. Tungsten and tungsten oxide sublimation

Multiple studies have reported that the oxidation of W to WO_3 forms volatile tungsten oxide species. These studies were conducted over a wide range of temperatures, from 773 K to 1920 K, and over a wide range of total pressures, from 0026 atm to 1 atm [16,19,20]. However, there are notable discrepancies. One study sates 1) tungsten oxides are volatile under high vacuum at 1073 K, and 2) WO_3 is not volatile in oxygen, argon, or high vacuum at 1273 K [21]. Lassner reports that $WO_{2(g)}$ forms more rapidly than $WO_{3(g)}$ at temperatures above 2100 K, and that tungsten metal will volatilize above 2500 K [22]. Lassner also states that WO_3 volatilization begins at temperatures as low as 873 K and volatilization rate increases dramatically above 1173 K [22]. The discrepancies found in literature on the volatility of tungsten oxides further demonstrate the historic difficulties in studying tungsten oxidation.

In an attempt to reconcile the issue of tungsten oxide volatility, a thermodynamic approach was taken. The equilibrium constants of the solid to gas sublimation reactions shown in Equation (18)–(20) were used to calculate the partial pressure of the gaseous oxides as a function of temperature at a constant pressure of 1 atm. Thermodynamic data for the gaseous species of the intermediate oxides, $WO_{2.72(g)}$ and $WO_{2.96(g)}$, were unavailable.

$$W_{(s)} \rightarrow W_{(g)} \tag{18}$$

$$WO_{2(s)} \rightarrow WO_{2(g)} \tag{19}$$

$$WO_{3(s)} \rightarrow WO_{3(g)} \tag{20}$$

After the partial pressures of the gaseous species were determined, their rate of sublimation was estimated using Langmuir's Evaporation Equation, shown in Equation (21), where dM/dt is the rate of sublimation, p is partial pressure of the vapor species, m is the mass of one particle, k is the Boltzmann constant, and T is temperature [23]. Estimated sublimation rates are plotted in Fig. 11.

$$\frac{dM}{dt} = p\sqrt{\frac{m}{2\pi kT}} \tag{21}$$

The estimated volatility of the tungsten species reaches as high as $1.5 \cdot 10^{-6}$ gcm^{-2} s^{-1} at 1643 K, the upper limit of temperatures considered for the thermodynamic cycle. At that rate, volatilization of the oxides is significant. At lower temperatures, however, the volatilization rate decreases substantially. At 1173 K, the volatility of WO_3 drops to $1.7 \cdot 10^{-13}$ g $cm^{-2}s^{-1}$, which is an acceptably low rate of volatilization and may explain why some studies have found that WO_3 is not volatile at temperatures in this range.

4.2. Volatilization in water vapor

Tungsten and tungsten oxides have shown high volatility rates when exposed to water vapor. The mechanism for volatilization has been determined to be due to the formation of a gaseous compound, $WO_3H_2O_{(g)}$ [24]. Lassner describes the formation of this species via reaction with tungsten metal or any of the tungsten oxides. These reactions have been provided in Equation (22)–(26) [22].

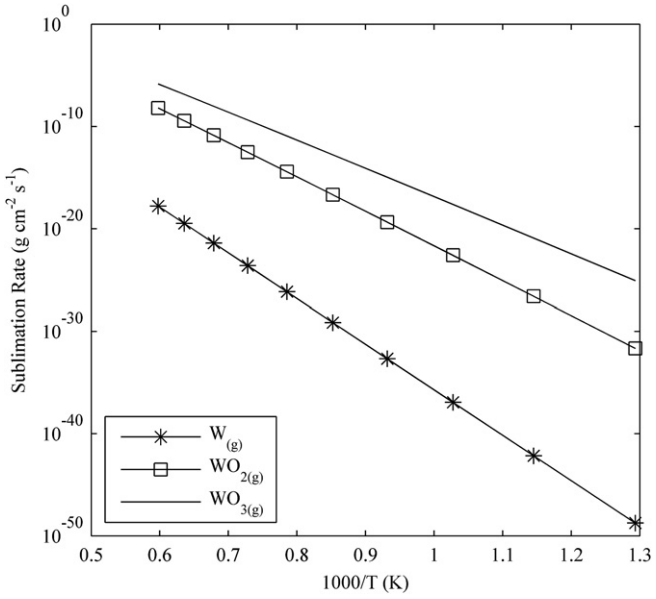

Fig. 11. Estimated sublimation rates of tungsten species as a function of temperature.

$$WO_{3(s)} + H_2O_{(g)} \rightarrow WO_3H_2O_{(g)} \tag{22}$$

$$10WO_{2.9(s)} + 11H_2O_{(g)} \rightarrow 10WO_3H_2O_{(g)} + H_{2(g)} \tag{23}$$

$$18WO_{2.72(s)} + 23H_2O_{(g)} \rightarrow 18WO_3H_2O_{(g)} + 5H_2O_{(g)} \tag{24}$$

$$WO_{2(s)} + 2H_2O_{(g)} \rightarrow WO_3H_2O_{(g)} + H_{2(g)} \tag{25}$$

$$W_{(s)} + 4H_2O_{(g)} \rightarrow WO_3H_2O_{(g)} + 3H_{2(g)} \tag{26}$$

Other studies have noted increased volatility rates when water vapor is present [25–27]. The study by Greene et al. presents a simple solution for the W/WO_3 syngas cycle by stating that the volatile hydroxide does not form at temperatures below 973 K. The study notes that the transition to volatilization in water vapor occurs between 973 K and 1073 K, which is the upper limit of the low temperature reaction [25]. Lassner adds some discrepancy to the matter by stating that the above 873 K, $WO_3H_2O_{(g)}$ is the most volatile tungsten species, however his ambiguity regarding temperatures maintains Greene's claims as plausible. A study by Warren et al. further backs the claim that volatilization by $WO_3H_2O_{(g)}$ formation does not occur at lower temperatures by having not detected the volatile species during tungsten oxidation in humid atmospheres up to 723 K [26].

5. Conclusion

The W/WO_3 redox cycle shows promise as a competitor for a solar to fuel conversion system for syngas production. When compared the ceria cycle, the W/WO_3 cycle shows much greater gravimetric fuel productivity and much higher solar to fuel conversion efficiencies. Due to the thermodynamic conditions of the system, the solar concentrator reactor will require two reaction chambers. In the first chamber, low temperature oxidation of tungsten by $H_2O_{(g)}$ will take place. $H_{2(g)}$ will be produced. This low temperature oxidation will occur at temperatures just below 973 K in order to avoid volatilization of tungsten and tungsten oxides in the presence of water vapor.

In the second reaction chamber, intermediate temperature oxidation of tungsten by $CO_{2(g)}$ will generate $CO_{(g)}$. This reaction will take place in the temperature range of 1073 K–1173 K. The reaction must take place above 1073 K in order for the reaction to be energetically favorable, and reaction temperatures will be limited to 1173 K to avoid rapid sublimation of tungsten and its oxides to the vapor phase.

Once the powder beds in both reaction chambers have completely oxidized, both chambers will be raised to a high temperature of 1173 K. $Ar_{(g)}$ will be used to decrease the pO_2 of both reaction chambers to form tungsten metal. Once the oxide powder bed has been completely reduced to metal, fuel production will begin again. The possible byproduct formation of tungsten carbide has also been considered, and the pCO/pCO_2 ratio will be maintained such that WC formation is not favorable.

References

[1] N.S. Lewis, D.G. Nocera, Proc. Natl. Acad. Sci. U. S. A. 103 (43) (2006) 15729–15735.
[2] W.C. Chueh, S.M. Haile, Thermochemical Synthesis of Fuels for Storing Thermal Energy, US7062320.
[3] W.C. Chueh, S.M. Haile, Philos. Trans. R. Soc. A 368 (2010) 3269–3294.
[4] T. Nakamura, Sol. Energy 19 (1976) 467–475.
[5] A. Steinfeld, Sol. Energy 78 (5) (2005) 603–615.
[6] S. Licht, Chem. Commun. (Cambridge, England) (37) (2005) 4635–4646.
[7] W.C. Chueh, C. Falter, M. Abbott, D. Scipio, P. Furler, S.M. Haile, A. Steinfeld, Science (New York, N.Y 330 (6012) (2010) 1797–1801.
[8] A. Steinfeld, Int. J. Hydrogen Energy 27 (6) (2002) 611–619.
[9] P.G. Loutzenhiser, A. Steinfeld, Int. J. Hydrogen Energy 36 (19) (2011) 12141–12147.
[10] K. Wegner, H. Ly, R. Weiss, S. Pratsinis, A. Steinfeld, Int. J. Hydrogen Energy 31 (1) (2006) 55–61.
[11] R. Haboury, U.B. Pal, P.A. Zink, S. Gopalan, S.N. Basu, Metall. Mater. Trans. B 43 (4) (2012) 1001–1010.
[12] S. Cifuentes, M. Monge, P. Pérez, Corros. Sci. 57 (2012) 114–121. December 2011.
[13] Outokumptu Research Oy, HSC Chemistry.
[14] O. Levenspiel, Chemical React. Engineering, third ed., Wiley, New York, 1999.
[15] D.S. Venables, M.E. Brown, Thermochim. Acta 285 (1996) 361–382.
[16] J.L. Sabourin, R. a. Yetter, J. Propul. Power 25 (2) (2009) 490–498.
[17] P.N. Walsh, J. Chem. Phys. 46 (9) (1967) 3571.
[18] G. Smolik, K. McCarthy, D. Petti, K. Coates, J. Nucl. Mater. 258-263 (1998) 1979–1984.
[19] E.A. Gulbransen, K.F. Andrew, J. Electrochem. Soc. 107 (7) (1960) 619–628.
[20] E. Gulbransen, K. Andrew, F. Brassart, J. Electrochem. Soc. 111 (1) (1964) 103–109.
[21] W.W. Webb, J.T. Norton, C. Wagner, J. Electrochem. Soc. 103 (2) (1956) 107.
[22] E. Lassner, W. Schubert, Tungsten: Properties, Chemistry, Technology of the Elem., Alloys, and Chemical Compounds, Kluwer Academic, New York, 1999.
[23] I. Langmuir, J. Am. Chem. Soc. 54 (7) (1932) 2798–2832.
[24] G. Belton, R. McCarron, J. Phys. Chem-US 33 (2) (1964) 1852–1856.
[25] G. Greene, C. Finfrock, Exp. Therm. Fluid Sci. 25 (2001) 87–99.
[26] A. Warren, A. Nylund, I. Olefjord, Int. J. Refract. Met. Hard. Mater. 14 (5–6) (1996) 345–353.
[27] F.J. Harvey, Metall. Trans. 5 (5) (1974) 1189–1192.